Comparison of a Barotropic Blocking Theory with Observation

J. G. CHARNEY

Massachusetts Institute of Technology, Cambridge, MA 02139

J. SHUKLA

Laboratory for Atmospheric Sciences, NASA/Goddard Space Flight Center, Greenbelt, MD 20771

K. C. MO

Sigma Data Services Corporation, Modeling and Simulation Facility, NASA/Goddard Space Flight Center, Greenbelt, MD 20771

(Manuscript received 4 September 1980, in final form 29 December 1980)

ABSTRACT

In an effort to explain observed blocking phenomena, the work of Charney and DeVore (1979) and Hart (1979) has been extended to incorporate observed zonal topography in a barotropic nonlinear channel model. Multiple stationary equilibria are obtained, one of which, for an appropriate forcing, corresponds exactly to the "normal" winter flow predicted by Charney and Eliassen (1949) from the linearized version of the model. When this forcing is applied in the nonlinear model, other equilibria, related to resonances with the wavenumber 2 and 3 Fourier components of the zonal topography, occur. Wavenumber 1 and 4 resonances could also have occurred with slight modifications of the model.

For comparison with observation, semi-objective criteria are adopted for identifying blocking events from daily 500 mb observations of 15 consecutive winter seasons. Following Dole (1978), we demand that there exist sufficiently large geopotential height anomalies for a sufficient length of time. Numerical values of the anomaly and duration criteria are determined from physical characteristics of observed blocks.

Altogether, 34 blocking events were found by this process, and the hemispheric patterns associated with 19 of these appear to be explainable qualitatively as one or another of the calculated equilibria. Five of the remaining blocking events might also have been explained if the forcing and geometry were somewhat altered.

What is not explained is the localized character of the blocking ridge (or trough) and the mechanism of transition to and from a blocking configuration. The failure to explain the localized properties is attributed in part to the exclusion of longitudinal variations of forcing and dissipation and in part to limitations on north–south structure in the model. It is suggested that the generation and decay of blocks may occur by changes of external factors driving the flow closer to or farther from topographic resonance, or by strong, large-scale cyclonic development. Another possibility is that when the flow is driven into a superresonant configuration, form-drag instability may transform it either into a subresonant blocking configuration or a nonblocking configuration.

1. Introduction

In a recent paper Charney and Devore (1979, hereafter referred to as CD) showed that given momentum and thermal sources acting on the fluid in a periodic β-plane channel with sinusoidal bottom topography may produce a multiplicity of stationary equilibrium states, and in particular that pure momentum forcing produces two stable states of which one resembles a weakly perturbed circumpolar vortex and the other the strongly perturbed blocking configuration. On this basis they suggested that blocking may be an alternate quasi-stable equilibrium state produced by the forcing of zonal flow over topographic, and perhaps thermal asymmetries of the lower boundary, and that transition from one equilibrium state to another may occur via a topographically induced form-drag instability.

It was not possible in CD to make comparisons with actual observations because one could not hope to obtain realistic patterns with purely sinusoidal topography. However, Hart (1979) showed that the truncated spectral equations obtained by CD could be derived merely by assuming that the cross-stream scale of the topography was large compared to the downstream scale. His equations became linear in the perturbation streamfunction and reduced to those of CD for sinusoidal topography, but because of the linearity are applicable to arbitrary downstream topographical variations.

Since actual topography does not have the large y scales postulated by Hart we have modified his model

0022-4928/81/040762-18$08.50

to obtain equations with arbitrary zonal variations of topography by projecting all variable functions onto the first topographic cross-stream mode: the topographic heights and streamfunctions are expanded as Fourier series in the cross-stream coordinate and the series are truncated after the first term. This accomplishes Hart's result but permits more realistic y variations in the topography (still not realistic enough, we hasten to add).

The advantage, if it may be deemed so, of the procedure adopted by Hart and ourselves is that it eliminates the self-interaction of the perturbation equations and therefore preserves the linearity of the perturbation equations. Indeed, the latter become just those used by Charney and Eliassen (1949, hereafter referred to as CE) in their analysis of topographically induced perturbations of a zonal flow at 500 mb. CE found it possible to account in a crude qualitative manner for the so-called "normal" flow pattern for the winter season in the vicinity of 45°N.

In the present case the mean zonal flow cannot be arbitrarily specified as it was in CE. It is determined by equilibrium among momentum forcing, form drag (mountain torque) and surface friction.

The present paper is the first in a two-part series. The second part will deal with a two-layer baroclinic channel flow, again with arbitrary zonal variations of topography. There, in place of the rather arbitrary momentum driving which must be assumed for the barotropic case, the zonal flow is driven thermally, and it becomes possible, as Derome and Wiin-Nielsen (1971) have shown in the linear case, to take into account asymmetric heat sources varying arbitrarily in the zonal direction.

To compare our results with those of Charney and Eliassen we choose the zonal momentum driving so as to give as one of the solutions of the nonlinear system of equations precisely the one obtained by CE. The momentum driving must then be such as to give the zonal flow, $U = 15$ m s^{-1}, the value used by CE. Actually it turns out that for this driving there are five possible solutions for U, only one of which is 15 m s^{-1}. Two of these lie on opposite sides of topographic wavenumber 2 resonance, two on opposite sides of topographic wavenumber 3 resonance, and the fifth is a zonal flow near the driving U^*. This last zonal flow is too large to be observed. The superresonant equilibrium solutions exhibit form-drag instability, but only for wavenumber 2 is the unstable growth rate so large as to preclude this equilibrium as a possible one. The superresonant wavenumber 3 equilibrium has an e-folding time of 28 days and therefore qualifies as a possible blocking configuration. The CE "normal" configuration corresponds to the stable subresonant wavenumber 2 solution.

A semi-objective method for locating observed blocking situations is described in the text. These are segregated visually into four classes corresponding to wavenumber 1, 2, 3 and 4 configurations. The wavenumber 2 and 3 configurations correspond to those we have found theoretically; the wavenumber 1 and 4 configurations have no counterpart in our calculations for the parameters used but could have if these parameters were varied; the remaining situations do not appear to fit our theory.

It will be seen that there is rather good correspondence with the calculated and observed 500 mb height fields except that the model does not simulate the regional character of the blocking pattern. It does not distinguish in amplitude among the main blocking ridge or ridges and the remaining downstream ridges which usually occur with considerably diminished amplitude. We think that this is due in part to the severe y truncation and in part to the failure to take into account longitudinal variations of the forcing function.

2. The barotropic model

The flow is assumed to be quasi-geostrophic and to take place in a β-plane channel with a rigid zero stress top. The governing potential vorticity equation,

$$\frac{\partial}{\partial t}\nabla^2\psi + J\left(\psi, \nabla^2\psi + \beta y + f_0\frac{h}{H}\right) = \frac{-f_0 D_E}{2H}\nabla^2(\psi - \psi^*), \quad (1)$$

is the same as that in CD for a rigid top. The quantity ψ is the quasi-geostrophic streamfunction, ψ^* the driving streamfunction, f_0 the Coriolis parameter $2\Omega \sin\Phi_0$ for the mean latitude Φ_0, $\beta = df/dy\big|_{\Phi=\Phi_0}$, h the perturbation height of the topography, H the mean height of the fluid and D_E the Ekman depth $(2\nu_e/f_0)^{1/2}$, where ν_e is a suitable bulk eddy viscosity.

A major simplification is obtained when the y Fourier series is truncated after the first term in the expansion of h. It is then reasonable to take the width of the β-plane channel as half the wavelength of the first topographic y mode. This makes the perturbations vanish at the zeros of the topography.

In contradistinction to CD, but in agreement with CE, we take the streamfunction as consisting of two parts, the first, $\bar{\psi}$, corresponding to top-hat profiles for U and U^* in which U and U^* are constant over the channel but vanish at its boundaries, and the second, ψ, a single Fourier sine series in y. This choice is made to permit a more realistic mean zonal velocity profile than would be given by a cosine profile whose wavelength corresponded exactly to that of the first topographic mode, since in reality the mean zonal velocity is determined by global thermal effects transcending the topographic height distribution alone. This formal device also yields a set of

equations which are identical to those of CE when one prescribes the mean zonal velocity. The zonal flow U produces a uniform Ekman transport which in our model demands side wall boundary layers and a return zero-stress boundary layer at the top, but, since the Ekman transport is constant, there is no horizontal friction layer divergence and therefore no influence on the internal motion. Alternatively, since side walls are an artificiality in our model, we might just as well have assumed that they are permeable to the uniform Ekman transport.

The x and y coordinates are scaled by L, where πL is the channel width, t by f_0^{-1}, ψ by $L^2 f_0$ and h by H. Then, in accordance with our assumptions, we set

$$\left.\begin{aligned} h &= h(x)\sin y \\ \psi &= -Uy + \phi(x, t)\sin y \end{aligned}\right\}.$$

Substitution of the above expressions in (1), multiplication by $\sin y$ and integration over the channel width gives

$$\frac{\partial}{\partial t}(\phi_{xx} - \phi) + U(\phi_{xxx} - \phi_x + h_x) + \beta\phi_x = -k(\phi_{xx} - \phi). \quad (2)$$

Similarly, multiplication of (1) by $\cos y$, integration over the channel width and integration with respect to x over the period of the channel gives

$$\frac{\partial U}{\partial t} = \tfrac{1}{3}\overline{(h\phi_x - \phi h_x)} + k(U^* - U), \quad (3)$$

where $k = D_E/2H$ and the overbar denotes an average value between $x = 0$ and $x = 2\pi R\cos\Phi_0/L$, where R is the radius of the earth. The factor 1/3 comes from the integral $\sin^2 y\cos y$. Eq. (3) shows that the fluctuations of zonal wind are determined by the relative magnitudes of the form drag, external driving and surface friction.

We note that Eq. (2) is similar to Eq. (34) of CE, except that U is not prescribed arbitrarily but is determined from (3). Since the form drag is determined by a product involving the topographic height and the perturbation streamfunction, it is now possible to have multiple equilibrium solutions depending on the amplitudes and phases of the forced stationary waves. The only arbitrary parameter in (3) is the value of the external driving. We have chosen this value so that one of the solutions corresponds exactly to the solution obtained by CE.

Following CE, we assume that the magnitude of the mean zonal velocity at the earth's surface is κ (=0.4) times its value at 500 mb, but have assumed that the perturbation is barotropic. The equations for stationary flow are then given by

$$U(\phi_{xxx} - \phi_x + \kappa h_x) + \beta\phi_x = -k(\phi_{xx} - \phi), \quad (4)$$

$$\tfrac{1}{3}\overline{(h\phi_x - \phi h_x)} = \kappa k(U - U^*). \quad (5)$$

3. Multiple equilibrium states in the presence of arbitrary zonal topography

The perturbation equation does not contain any nonlinear terms because the self-interaction terms vanish and topography and perturbations have only $\sin y$ variations in the meridional direction. It is therefore possible to take an arbitrary zonal profile of the mountains and calculate the equilibrium solutions from (4) and (5).

By substituting

$$\phi = \sum_{n=1}^{\infty}(a_n\cos n\alpha x + b_n\sin n\alpha x),$$

$$h = \sum_{n=1}^{\infty}(h_{nc}\cos n\alpha x + h_{ns}\sin n\alpha x),$$

[where $\alpha = L/(R\cos\Phi_0)$], in Eqs. (4) and (5), we derive the following expressions for a_n and b_n:

$$a_n = \frac{1}{k^2 + n^2\alpha^2\left(U - \dfrac{\beta}{1 + n^2\alpha^2}\right)^2}\left[\frac{Un\alpha\kappa k}{1 + n^2\alpha^2}h_{ns} + \frac{Un^2\alpha^2\kappa\left(U - \dfrac{\beta}{1 + n^2\alpha^2}\right)}{1 + n^2\alpha^2}h_{nc}\right],$$

$$b_n = \frac{1}{k^2 + n^2\alpha^2\left(U - \dfrac{\beta}{1 + n^2\alpha^2}\right)^2}\left[\frac{-Un\alpha\kappa k}{1 + n^2\alpha^2}h_{nc} + \frac{Un^2\alpha^2\kappa\left(U - \dfrac{\beta}{1 + n^2\alpha^2}\right)h_{ns}}{1 + n^2\alpha^2}\right]. \quad (6)$$

The equilibria are determined from

$$U^* - U = F(U), \quad (7)$$

where

$$F(U) = \frac{1}{3}\sum_{n=1}^{\infty}\frac{n^2\alpha^2}{1 + n^2\alpha^2} \times \left[\frac{U(h_{nc}^2 + h_{ns}^2)}{k^2 + n^2\alpha^2\left(U - \dfrac{\beta}{1 + n^2\alpha^2}\right)^2}\right]. \quad (8)$$

In practice the sum appearing in the above equations is truncated at $n = N$ where $N = 35$.

Following CE we have chosen the width of the channel (πL) to be 33° of latitude and the mountain profile to be the average of observed mountain heights at latitudes 42, 46 and 50°N. The mountain heights at these latitudes were first obtained by averaging the earth's topography with 1° × 1° resolution. In CE the h profile in Eq. (2) was obtained by averaging at latitudes 40, 45 and 50°N. The mountain profile used in this study and shown in Fig. 1 is very similar

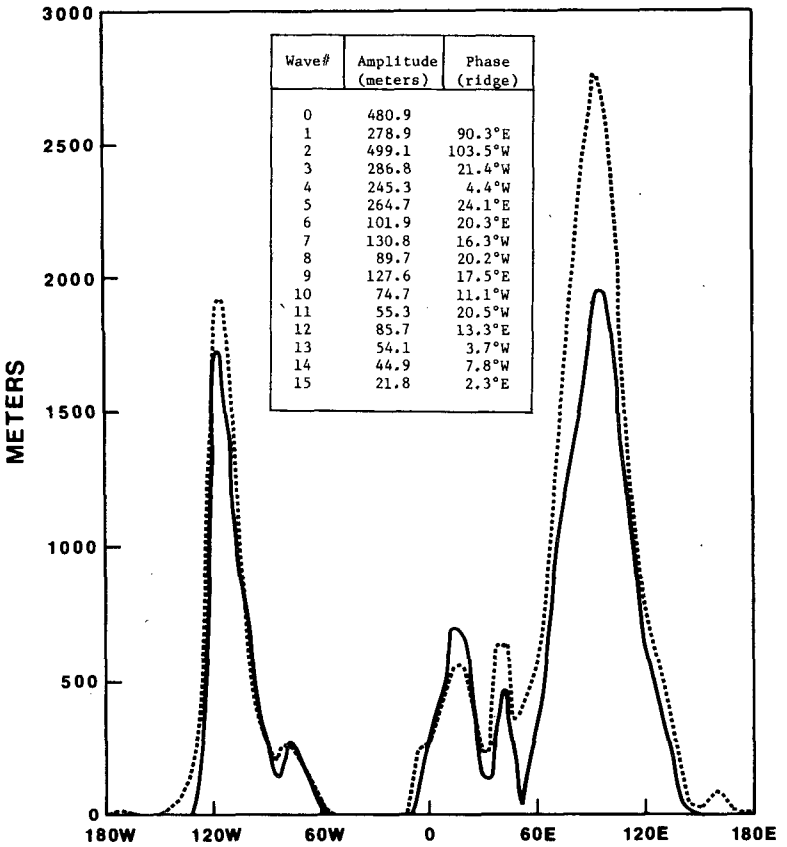

FIG. 1. Earth's topography and its zonal wavenumber decomposition. The dashed line is obtained by topographic projection onto a siny profile between 30 and 62°N.

to this profile. The phases and amplitudes of the Fourier components of the topography are shown in the inset table to Fig. 1. We realize that it would have been more consistent to have projected the mountain heights onto a siny profile between $y = 0$ at 30°N and $y = \pi$ at 62°N. This was not done because we wished to obtain agreement with CE. The latter profile is shown as the dashed line in Fig. 1.

Since the time is scaled by f_0^{-1} ($f_0 = 1.011 \times 10^{-4}$ s^{-1}) and the length by L (1.167×10^6 m), the velocity is scaled by Lf_0 (=117.98 m s^{-1}). The value of the nondimensional β, $L/(R \cot\Phi_0)$ is 0.1835 and $\alpha = L/R \times \cos\Phi_0 = 0.260$. The depth of the fluid and the height of the mountains is scaled by H (=8 km). We have calculated the equilibrium solutions for $N = 35$ and various choices of k. For nondimensional $k = 0.008$ Eq. (4) is identical to Eq. (34) of CE, and since we have chosen U^* such that one of the solutions is identical to CE, we present here the results for $k = 0.008$. This corresponds to the bulk eddy viscosity $\nu_e = 5.2$ m^2 s^{-1}.

Fig. 2 plots $F(U)$ against U nondimensionally. $F(U)$ for the alternative h profile of Fig. 1 is shown as a dashed line. We note from Eq. (8) that $F(U)$ tends to have resonant peaks at $U = \beta/(1 + n^2\alpha^2)$; however, for $n = 1$, friction is so large that this peak does not appear. The value $U = 0.128$ corresponds to 15 m s^{-1}, chosen by CE to calculate the stationary response. From Eq. (7), $U = 0.128$ gives $U^* = 0.53$ which corresponds to the straight line in Fig. 2. It is seen that this straight line intersects $F(U)$ at five points. $U = 0.128$, corresponding to the CE solution, is the subresonant wavenumber 2 equilibrium and $U = 0.163$ is the superresonant wavenumber 2 equilibrium. Similarly $U = 0.113$ and 0.120 are respectively the subresonant and superresonant wavenumber 3 solutions. The strongly superresonant wavenumber 1 solution appears at $U = 0.526 \approx U^*$ and is quite unattainable in the geometry of our model. However, for other geometries, i.e., a smaller lateral extent, the strongly superresonant wavenumber 1 equilibrium might be permitted, and for a smaller k both wavenumber 1 and 4 resonances come into play. It should also be remarked that when the equilibrium U is close to a resonance, the solution is dominated by the corresponding Fourier component of the topography, but that in general all components have some effect.

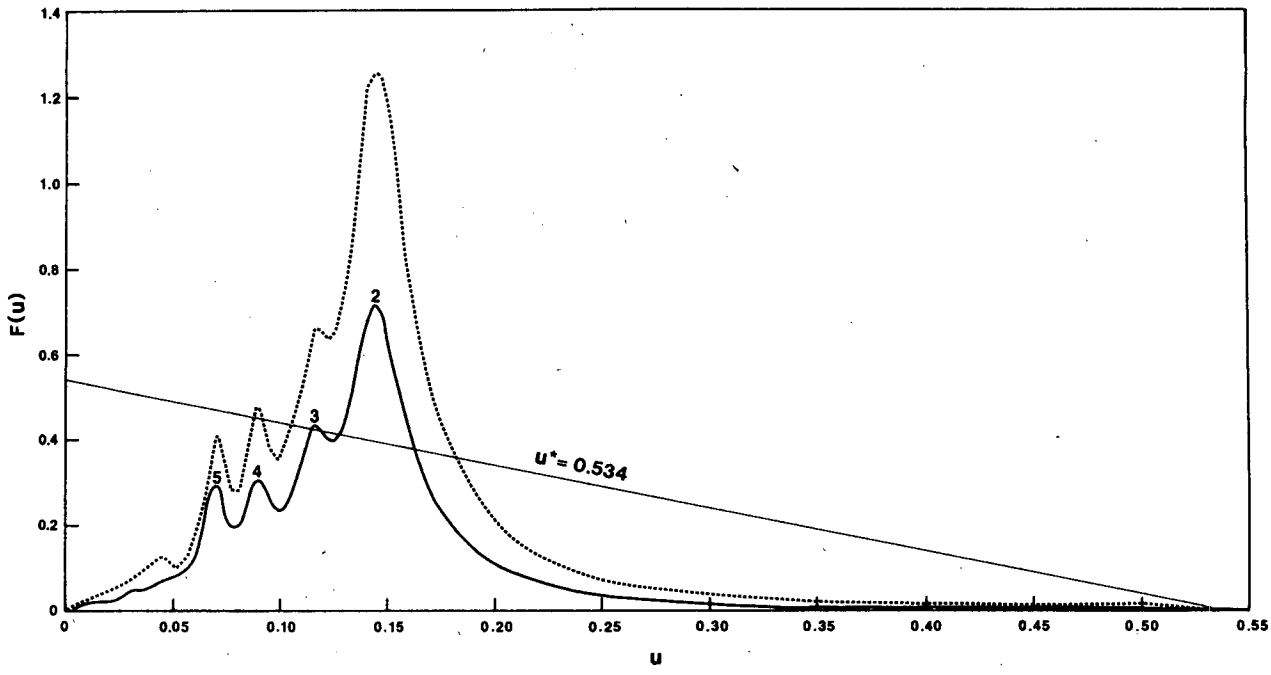

FIG. 2. Nondimensional $F(U)$ versus U. The integers at the peaks indicate the resonant topographic wavenumbers. The straight line corresponds to constant value of $U^* = 0.534$; the dashed line gives $F(U)$ for the dashed topographic profile of Fig. 1.

Figs. 3 and 4 give the structure of the equilibria for wavenumbers 2 and 3, respectively. Fig. 3 also shows the normal observed pattern for January. The subresonant wavenumber 2 solution is identical to that of CE (Fig. 4 in CE for $\sigma = 0.25$). This closely corresponds to the normal, non-blocking, wintertime circulation pattern, which is shown as the dotted curve in Fig. 3. However, when the driving is increased, the flow approaches closer to resonance and the perturbation amplitude becomes larger and thus begins to resemble a blocking situation. The superresonant wavenumber 2 solution shows an intensified ridge along 120°W and a rather deep Aleutian trough along 160°E. These are, at times, pronounced features of blocking over the west coast of the United States; however, the corresponding configuration over the Atlantic and Europe does not appear to resemble any observed persistent pattern. Among the four equilibria, this is the most unstable (shown in the next section) and it must be precluded as a possible equilibrium state at least for the barotropic model. The subresonant and the superresonant wavenumber 3 equilibria are similar in structure, the major troughs and ridges in the superresonant solution being displaced between 10 and 20° eastward from those in the subresonant solution. Although the difference in the intensity of the major troughs and ridges in the two cases is not large, it is interesting to note that in the subresonant solution the Aleutian trough (longitude 140°E) is the deepest and the downstream ridge the strongest, a feature commonly observed during Pacific blocking, whereas in the superresonant solution the deepest trough is along 80°W and the strongest ridge along 10°W, and this is observed in the European blocking patterns shown in the examples of Section 5.

4. Stability analysis

We now examine the stability of the equilibrium solutions. For

$$\left.\begin{aligned} U(t) &= U_0 + U'(t) \\ \phi(x, y, t) &= \phi_0(x, y) + \phi'(x, y, t) \end{aligned}\right\},$$

where subscript zero denotes the equilibrium solution and the primes denote the perturbations, the linearized perturbation equations derived from (2) and (3) become

$$\frac{\partial}{\partial t}(\phi'_{xx} - \phi') + U_0(\phi'_{xxx} - \phi'_x) + U'(\phi_{0xxx} - \phi_{0x} + \kappa h_x) + \beta\phi'_x = -k(\phi'_{xx} - \phi'), \quad (9)$$

$$-\frac{\partial U'}{\partial t} + \tfrac{1}{3}\overline{(h\phi'_x - \phi' h_x)} = \kappa k U'. \quad (10)$$

Assuming the time variation to be $e^{\sigma t}$, where σ is complex ($\sigma = \sigma_r + i\sigma_i$), and substituting

$$\left.\begin{aligned} \phi_0(x, y) &= \sum_{n=1}^{\infty} (a_{n0} \cos n\alpha x + b_{n0} \sin n\alpha x) \\ \phi'(x, y, t) &= \sum_{n=1}^{\infty} [a'_n(t) \cos n\alpha x + b'_n(t) \sin n\alpha x] \end{aligned}\right\},$$

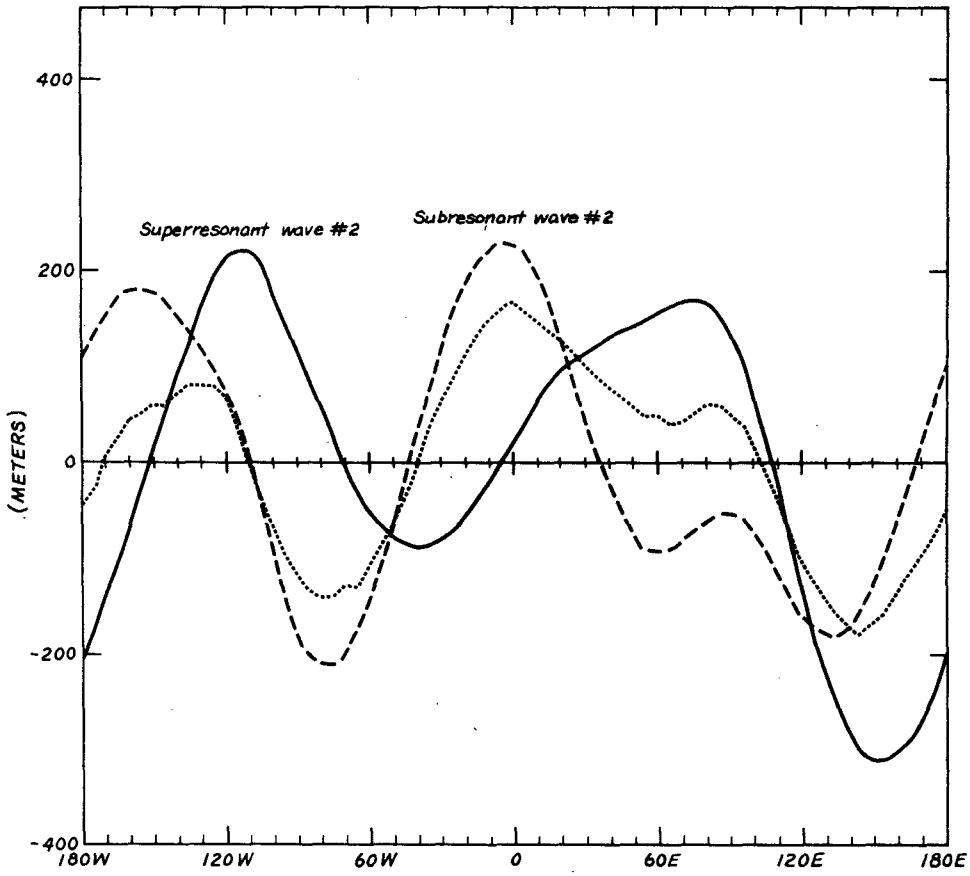

FIG. 3. Subresonant and superresonant wavenumber 2 solutions. The normal January departure of the 500 mb geopotential height field from the zonal mean is shown as the dotted curve.

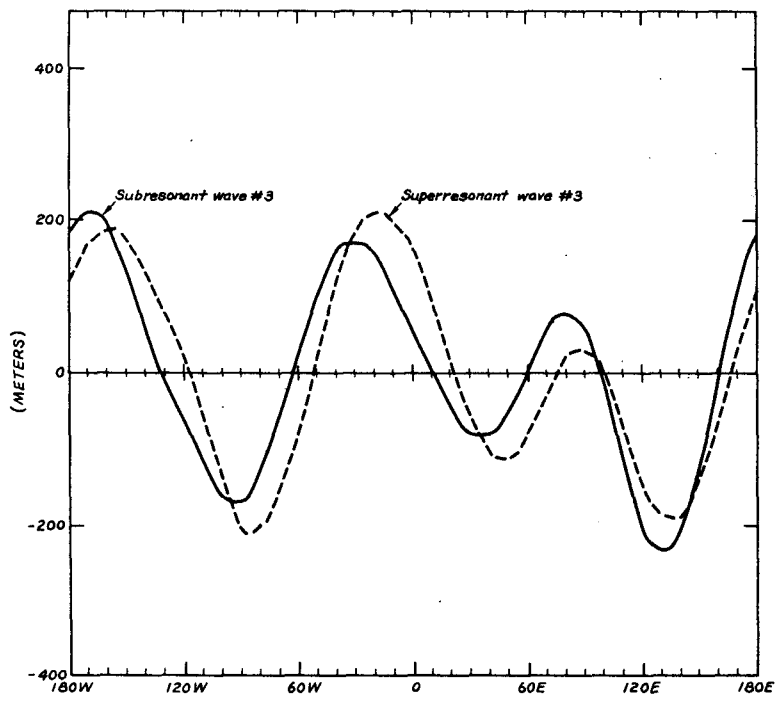

FIG. 4. Subresonant and superresonant wavenumber 3 solutions.

TABLE 1. Stability analysis of equilibrium solutions.

U (non-dimensional)	n wave-number	U (m s^{-1})	σ (non-dimensional)	e-folding time (days)
0.113	3	13.2	0.0001316 $\pm$ 0.02488i	870
0.120	3	14.0	0.00406	28
0.128	2	15.0	0.0	∞
0.163	2	19.1	0.01945	6

Eqs. (9) and (10) are reduced to a single equation in σ of order $(2N + 1)$

$$3(\sigma + \kappa k) = (\sigma + k) \sum_{n=1}^{\infty} \times \left[\frac{n^2\alpha^2(b_{n0}h_{ns} + a_{n0}h_{0c}) - \kappa\left(\frac{h_{nc}^2 + h_{ns}^2}{1 + n^2\alpha^2}\right)}{(\sigma + k)^2 + n^2\alpha^2\left\{U_0 - \frac{\beta}{1 + n^2\alpha^2}\right\}^2} \right] + \sum_{n=1}^{\infty} \left[\frac{n^3\alpha^3\left(U_0 - \frac{\beta}{1 + n^2\alpha^2}\right)(a_{n0}h_{ns} - b_{n0}h_{nc})}{(\sigma + k)^2 + n^2\alpha^2\left\{U_0 - \frac{\beta}{1 + n^2\alpha^2}\right\}^2} \right]$$

Since we are mainly concerned with the fastest growing modes, we have shown in Table 1 the solutions corresponding to the largest positive values of σ_r.

It is seen that the subresonant wavenumber 2 equilibrium which corresponds to the normal winter pattern of CE is stable. The subresonant wavenumber 3 solution is very weakly unstable, and the perturbation has a period of about 10 days. Normally, one expects stability on the subresonant side for purely sinusoidal topography, but as one of the reviewers of this paper has remarked, other topographic components might come into play. However, we do not understand why the instability appears as a traveling wave. The superresonant wavenumber 2 and 3 solutions exhibit the form-drag instability, which grows in place. The e-folding time for the superresonant wavenumber 3 equilibrium is large enough (28 days) to be considered as a possible equilibrium state.

5. Comparison with the observations

There has been considerable diversity in the criteria for identification of blocking events from observed data. The two most important elements of all criteria have been the kinematic structure of the flow pattern and its persistence in time. Earlier criteria (*viz.*, Rex, 1950) have focused attention both on shape and on persistence, but since the simplicity of the current model makes comparisons of detailed structure difficult, we have considered only the persistence criteria as a means of objective identifications of blocking anomalies from the observations. However, we remark that the blocking events so selected do correspond in structure with the definitions of Rex and others in nearly every case. According to the criteria used by Dole (1978), a blocking event is identified by persistence of an anomaly of one standard deviation (~100 gpm) or greater for 10 days or more. The choice of 100 gpm and 10 days, though reasonable, is somewhat arbitrary. Therefore, we have examined the daily data to see if these data suggest a less arbitrary way of choosing the actual values of the threshold values.

We have examined the observed daily geopotential height fields for 500 mb for 15 winter seasons (1963–77). First, we calculated the ensemble mean time series by averaging all the available data for each calendar date. We then determined the mean winter seasonal cycle by fitting a parabola ($a + bt + ct^2$) to the ensemble mean time series for 90 days (1 December–28 February). The difference between the observed values and the mean seasonal cycle is referred to as the anomaly field for the 500 mb geopotential height. The daily anomaly field was calculated for a 5° × 5° grid resolution over the Northern Hemisphere between 20 and 90°N for the 15 winter seasons.

We then prepared time-longitude cross sections at 50, 60 and 70°N for these daily values of the anomalies. An examination of the cross sections revealed that there were several anomalous events along longitude bands of width 15–30°. Fig. 5 shows the plot of the total number of days for which, during the 15 winter seasons, at each grid point along 50°N, an anomaly greater than +200 gpm persisted for more than 7 days. The reason for choosing this criterion is explained below.

Persistent positive anomalies show two major preferred locations, between longitudes 180 and 130°W and 55 and 0°W. There also were several anomalies which persisted but also exhibited a tendency to propagate slowly. Westward propagation was more dominant at 60 and 70°N than at 50°N where eastward propagation occasionally could be seen.

In order to identify the instances of observed blocking events, we asked the two following questions:

(i) Is there a significant preference for the occurrence of anomalies of certain magnitudes?

(ii) Is there a relationship between the size of the anomaly and its duration?

In order to examine the first question, we calculated the frequency of occurrence of anomalies (Fig. 6). To do this we combined the data for 360 grid points (72 grid points each at 50, 55, 60, 65 and 70°N) and 1319 days [59 days (January–February) in 1963 and

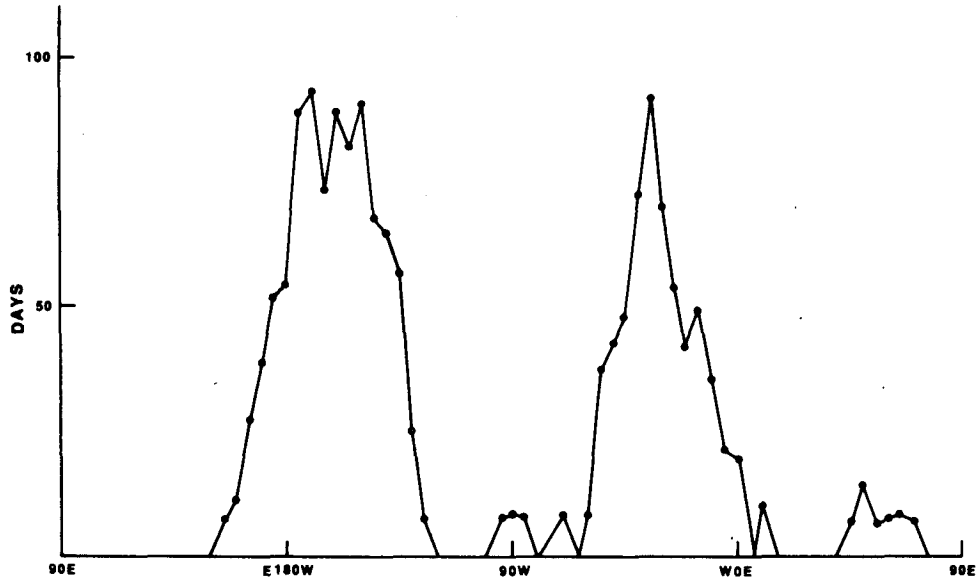

FIG. 5. Total number of days for which the 500 mb geopotential height anomaly ≥ 200 gpm persisted for 7 days or more.

90 days (December–January–February) each for the 14 years, 1964–77]. Thus 474 840 samples were used for this figure. It should be pointed out that all the samples are not independent because the atmospheric anomalies have characteristic space and time scales. Frequencies of occurrence were calculated for an anomaly range of 50 gpm. Thus in Fig. 6, the frequency plotted against the anomaly value of ±25 gpm, refers to the total number of all the points for which anomaly was between 0 and 50 gpm. It is seen that the frequency is a maximum for the smallest anomaly and decreases for larger anomalies. The shape of the curve remains essentially unchanged if the grid points are chosen only for the selected longitude sectors (180–130°W) and 55°W–0°E), the preferred sectors of blocking. It is seen that for the smaller magnitudes the negative anomalies are more frequent than the positive anomalies, whereas for the larger magnitudes the positive anomalies are more frequent than the negative anomalies. Fig. 7 shows the total contribution of an anomaly of a given magnitude (product of frequency and magnitude) for positive and negative anomalies. By definition of the anomaly, the area under each curve is equal. It is seen that the negative anomalies dominate for the magnitudes of 225 gpm and less and positive anomalies dominate for the magnitudes 275 gpm and more. In both the cases the maximum contribution to the total anomaly comes from the anomalies of magnitude 175 ± 25 gpm. On this basis we have chosen 200 gpm as a threshold for determining a blocking event.

In order to examine the second question we have calculated the frequency of occurrence of anomalies ≥ +200 gpm and ≤ −200 gpm which persisted for certain number of days. Fig. 8 shows the plot of the total number of days (product of frequency and days) versus the number of days of persistence. The maximum value occurs for 2 days, which corresponds to medium-scale traveling disturbances. Although

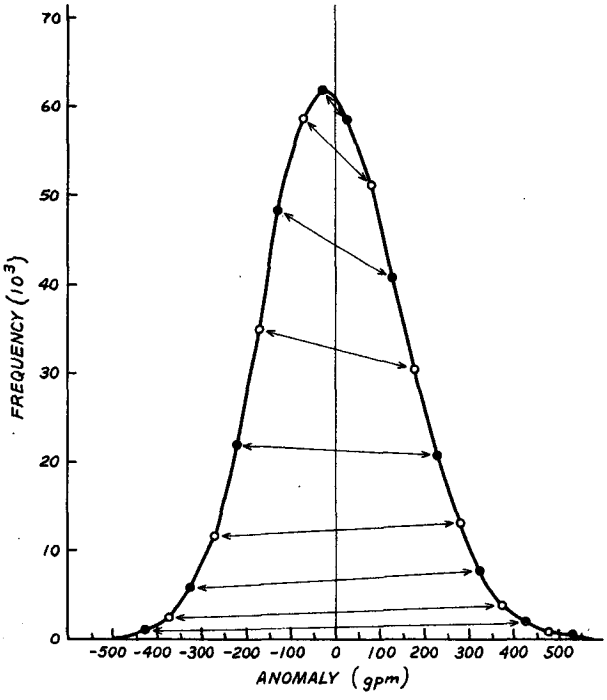

FIG. 6. Frequency of occurrence of daily 500 mb geopotential height anomaly.

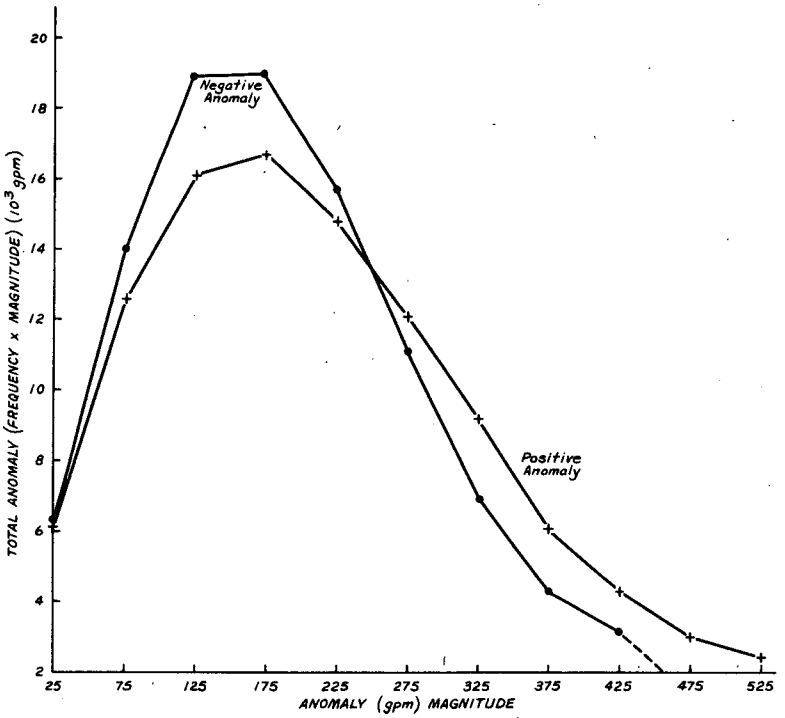

FIG. 7. Total contribution of positive and negative anomalies as a function of magnitude of the anomaly.

there is no secondary maximum either in the frequency diagram (not shown) or in the plot of total number of days (frequency × duration days), for anomalies ≥ 200 gpm there is a break in the curve suggesting another process that occurs around 7–8 days. For anomalies ≤ -200 gpm (not shown), a similar slope discontinuity occurs at 9 days. The diagram (not shown here) based only on the preferred regions of blocking (180–130°W and 55°W–0°E) shows an actual maximum at 9 days. On the basis of these considerations, a threshold in the range of 7–10 days seems to be appropriate. These values

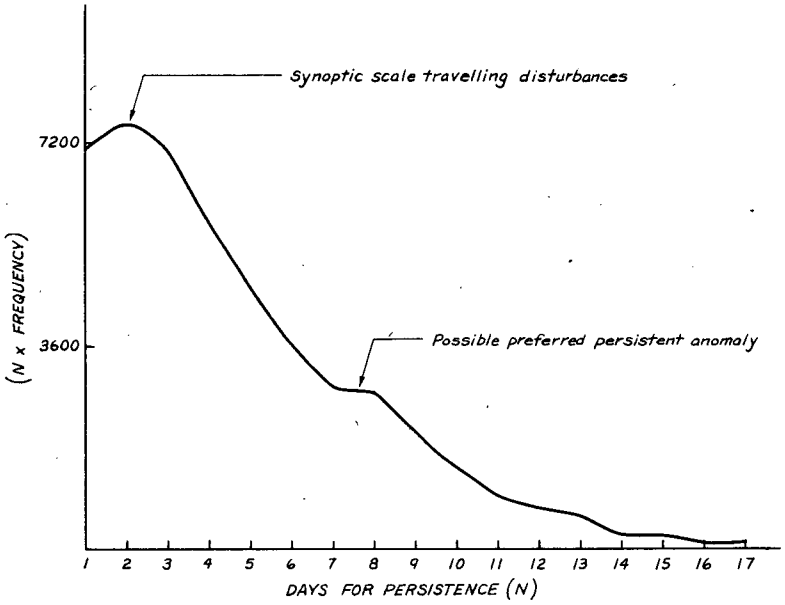

FIG. 8. Product of frequency and days versus number of days of persistence.

did not change with a change of the threshold criterion for the height anomaly from 200 to 100 gpm.

A subjective determination of the dates of the beginning and end of each blocking event was considered more appropriate than an objective determination because it enabled us to take into account the spatial coherence and tendency toward propagation of an anomaly pattern. As already mentioned, we have noticed that there are a few instances of slowly westward propagating global wave patterns which are associated with the amplification of a blocking ridge. The most remarkable example occurred in the winter of 1976–77, when the preexisting ridge along the west coast of the United States was periodically reintensified by westward propagating long waves of period of ~15 days. The westward propagation was more prominent at 60 and 70°N than to 50°N (see Fig. 9). A possible explanation of this phenomenon may be contained in the paper of Charney and Straus (1980) where it is shown that a given baroclinic blocking pattern may be unstable to periodic or quasi-periodic disturbances propagating westward with periods of the order of 15 days.

Table 2 gives a list of events chosen from an examination of the time-longitude cross sections of daily anomalies at 50°N for 15 winter seasons. This table includes all those events for which a positive anomaly of 200 gpm or more persisted for 10 days or more. Persistence of an anomaly by itself does not guarantee the persistence of a ridge. For example, if the intensity of the Aleutian low is very weak compared to normal, it may show a large positive anomaly and a weaker seasonal ridge may show a negative anomaly. Thus the simultaneous occurrence of a positive anomaly over the Aleutian low and a negative anomaly over the west coast of North America can be associated with a stronger zonal flow rather than a blocking configuration. We examined each of the 14 events separately and in each case a pronounced ridge was indeed present. These events were then visually segregated by similarities in the locations of major troughs and ridges.

TABLE 2. List of events which a positive anomaly of 200 gpm or more persisted for 10 days or more.

1. 17–28 Feb 1972	8. 25 Dec–6 Jan 1968
2. 1–14 Dec 1972	9. 17 Dec–6 Jan 1965
3. 31 Dec–10 Jan 1974	10. 23 Dec–1 Jan 1966
4. 27 Jan–12 Feb 1975	11. 31 Dec–14 Jan 1969
5. 8–30 Jan 1963	12. 15 Jan–2 Feb 1971
6. 3–19 Feb 1965	13. 21 Dec–2 Jan 1968
7. 5–14 Jan 1967	14. 10–22 Feb 1969

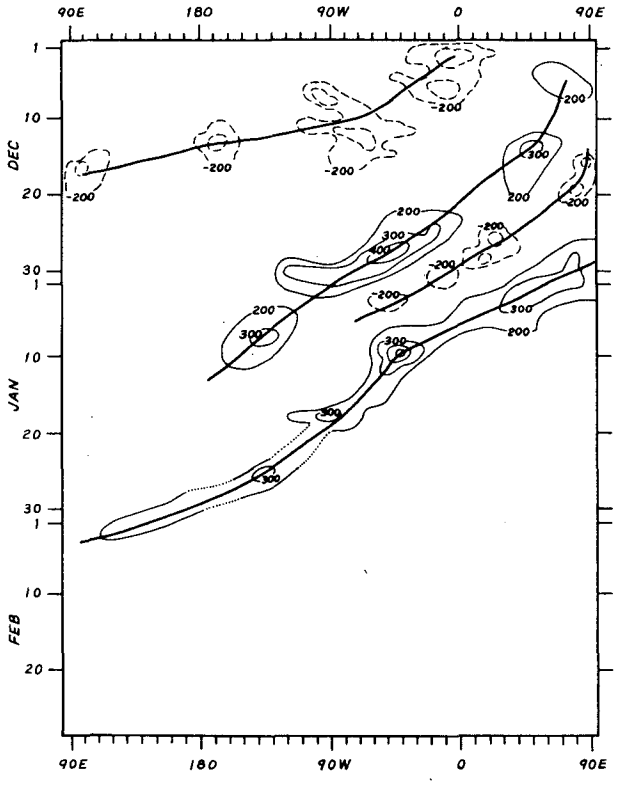

FIG. 9. Time-longitude cross section of 500 geopotential height anomaly for 1976–77 winter season.

In the following, we have chosen to represent observed patterns as deviations from the zonal average rather than as climatological anomalies, for only the former are physical entities which may be directly compared to calculations.

Figs. 10 and 11 give the plots of the 500 mb geopotential height field (departures from zonal mean) averaged for 50, 55 and 60°N and in time for each of the first eight events. The heavy solid line in each figure is the average of all the events. Fig. 10 is characterized by the presence of two major troughs and two major ridges and is very similar to the normal winter pattern suggested by CE as due to orographic forcing. This suggests that some blocking events are simply an amplification of the normal pattern. Fig. 10 should be compared to the Fig. 3, which shows the stable subresonant wavenumber 2 configuration and corresponds to the CE "normal" configuration. It will be seen that there are strong resemblances.

Fig. 11 is characterized by the presence of three troughs and three ridges. The trough along 30°E and the neighboring ridge along 80°E are not as intense as the other two troughs and ridges. This pattern is similar to the superresonant wavenumber 3 equilibrium shown in Fig. 4. There is some discrepancy in the phases of the first ridge along 140°W and second trough along 30°E which in the analytical solutions are displaced by 20° westward and eastward, respectively. The subresonant and superresonant wavenumber 3 solutions are similar in structure except that the phases of the major troughs and ridges in the former are displaced between 10 and 20° westward compared to the latter.

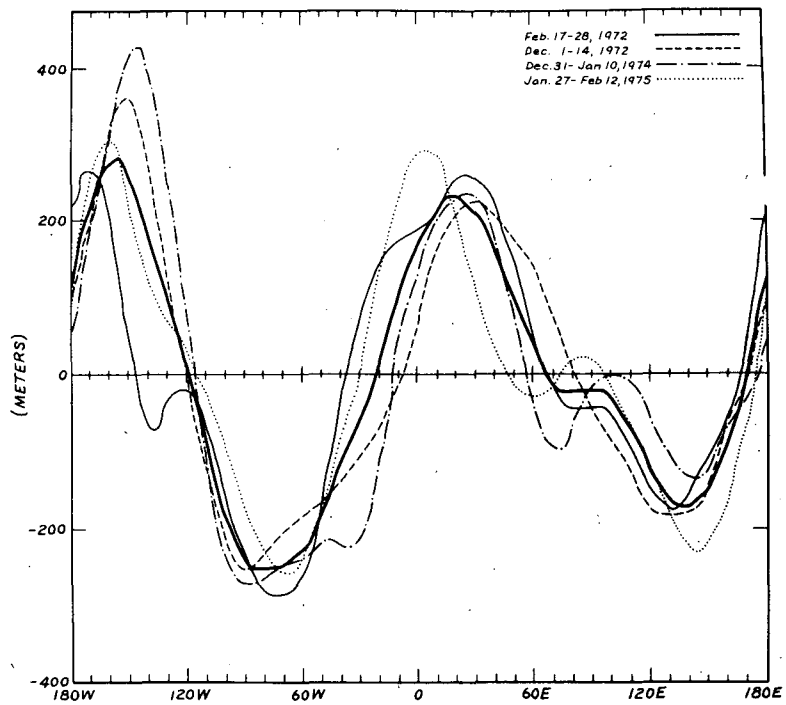

FIG. 10. Departure from zonal mean of observed 500 mb geopotential height averaged for 50, 55, 60°N and in time for the duration of each event. The persistence criteria was 10 days or more and these are similar to wavenumber 2 solutions.

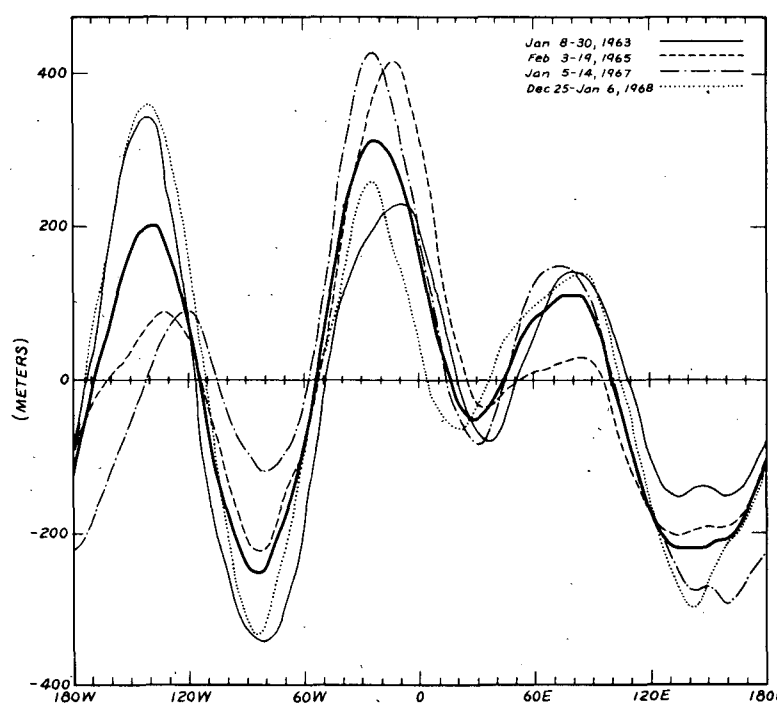

FIG. 11. As in Fig. 1 but similar to wavenumber 3 solution.

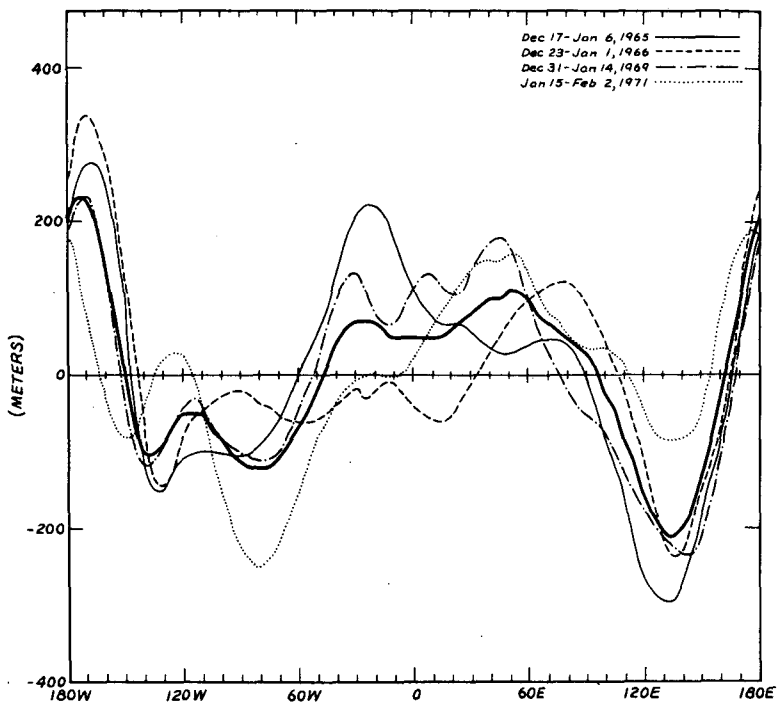

FIG. 12. As in Fig. 10 without analytical counterpart.

Figs. 12 and 13 give plots of the other blocking events of Table 2 for which we have not found analytical counterparts. Since the present model is highly simplified (severe y truncation and no role for longitudinally variable forcing), one cannot expect it to explain all the blocking events.

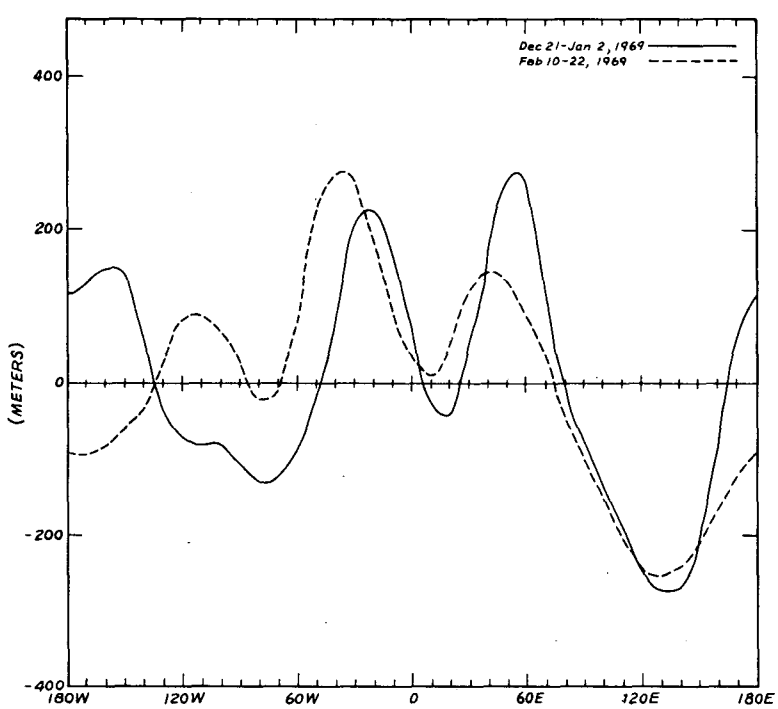

FIG. 13. As in Fig. 10 without analytical counterpart.

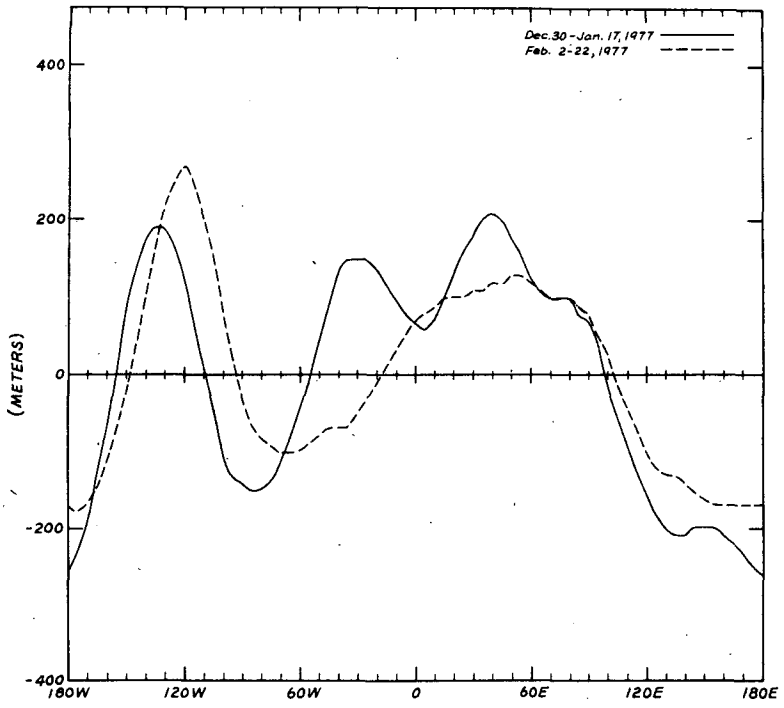

FIG. 14. As in Fig. 10 except that the negative anomaly of −200 gpm or less persisted for 10 days or more.

If the criteria for choosing a blocking event had been the persistence of a negative anomaly of −200 gpm or less for 10 days or more, the only two events which are not already included in Table 2 are those for 30 December 1976–17 January 1977 and 2–22 February 1977. This is so because during the winter of 1976–77, the Aleutian low was unusually intense and the downstream blocking ridge was coincident with the normal seasonal ridge at 50°N. The positive departures over the ridge were therefore not as large as the negative departures over the Aleutian low. Fig. 14 gives the plots of these two events. For the 30 December 1976–17 January 1977 event there is no analytical counterpart; however, the 2–22 February 1977 event has a close resemblance to the superresonant wavenumber 2 solution. Since this solution is topographically unstable (form drag instability) with an e-folding time of only 6 days, it is not expected to persist for longer periods and therefore its observed persistence points to the limitations of the present model. It is well known, however, that during the winter of 1976–77, there were unprecedentedly large sea surface temperature anomalies in the Pacific ocean and it is quite possible that diabatic heat sources were important factors in the blocking events during that season (Namias, 1978; Shukla and Bangaru, 1980).

TABLE 3. List of additional events of persistent anomaly.

1. 7–13 Jan 1971	11. 6–12 Jan 1977
2. 25 Jan–1 Feb 1971	12. 6–13 Dec 1964
3. 3–9 Jan 1973	13. 13–25 Dec 1972
4. 22–29 Jan 1963	14. 11–25 Jan 1970
5. 29 Jan–4 Feb 1963	15. 4–10 Dec 1967
6. 1–10 Feb 1964	16. 11–24 Jan 1968
7. 25 Dec–22 Jan 1968	17. 1–7 Dec 1966
8. 24 Jan–1 Feb 1968	18. 6–12 Feb 1968
9. 1–9 Dec 1969	19. 17–25 Dec 1971
10. 2–9 Feb 1971	20. 11–28 Dec 1974

Table 3 gives the additional blocking events that could be identified from an examination of the time-longitude sections by reducing the persistence criterion from 10 to 7 days. If two or more successive 7-day events were discontinued for only one or two days, we combined them to form a single event. These events were again segregated according to their structure as described earlier. Fig. 15 gives the plots of all the events that are similar to the normal winter configuration and Fig. 16 gives the plots of those events that closely resemble the superresonant wavenumber 3 configuration. It is remarkable that even for the reduced criterion for the duration of blocking, many of the observed blocking events resemble equilibrium states of the barotropic model with realistic topography along a latitude circle.

For convenience of comparison we have shown the average of Fig. 10, the average of Fig. 15, and the subresonant wavenumber 2 configuration together in Fig. 17. Similarly, in Fig. 18, we have shown the

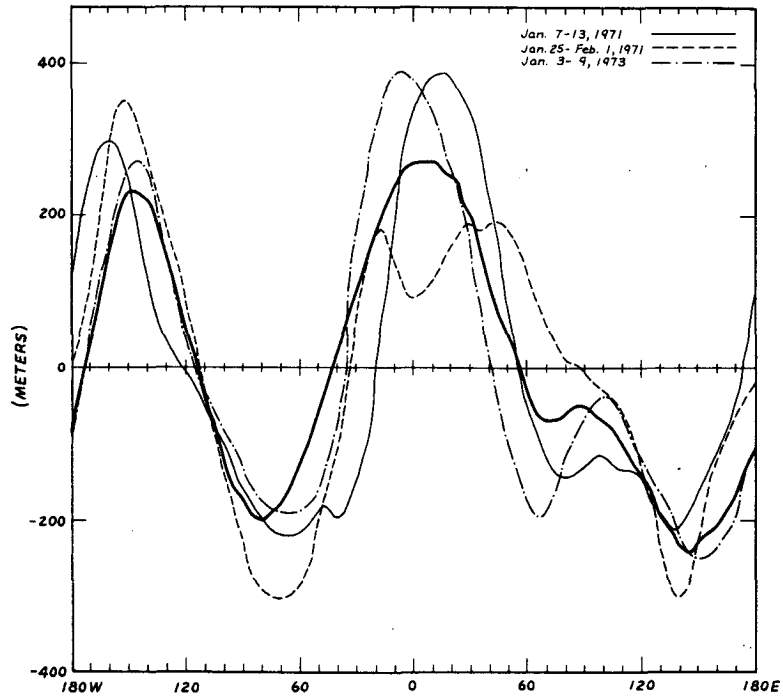

FIG. 15. As in Fig. 10 except for persistence criteria of 7 days or more. These are similar to the wavenumber 2 solution.

average of Figs. 11 and 16, and the subresonant and the superresonant solutions for wavenumber 3. These figures suggest that, despite the simplicity of the model, the analytical solutions closely resemble large numbers of observed blocking configurations.

Figs. 19 and 20 show the events listed in Table 3

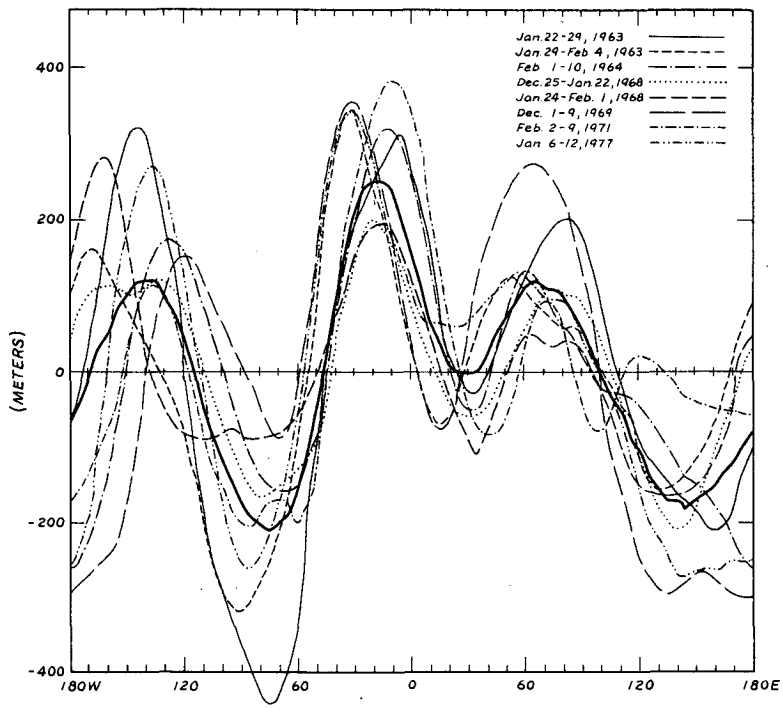

FIG. 16. As in Fig. 15 but similar to wavenumber 3 solutions.

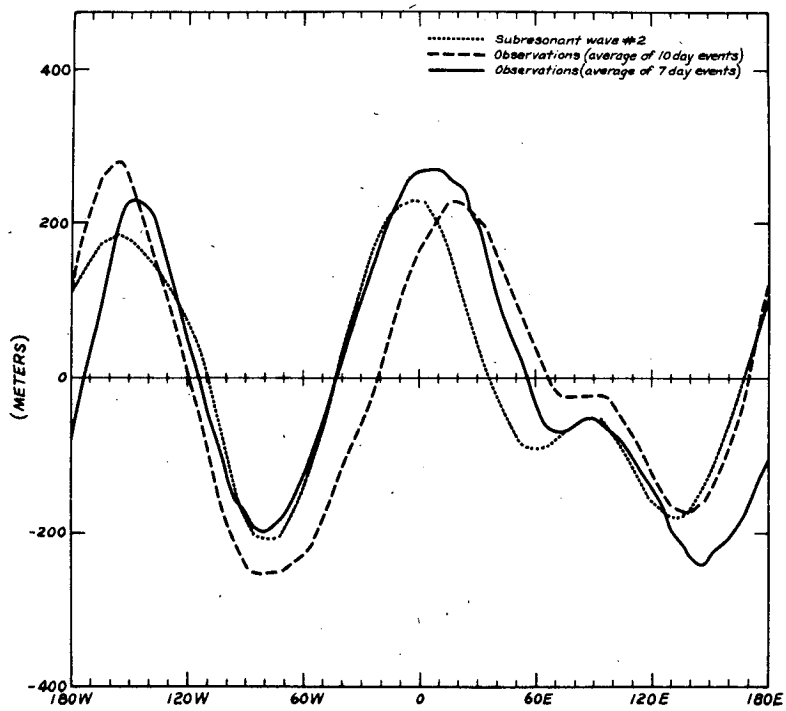

FIG. 17. Subresonant wavenumber 2 solution and average of all events in Figs. 10 and 15.

that are dominated by wavenumbers 1 and 4, respectively. For the prescribed driving, we have not found analytical solutions which correspond to wavenumbers 1 and 4 equilibria. However, if friction were reduced or if the external driving were reduced from 0.53 to 0.40 (nondimensionally), this model would have given wavenumber 4 equilibria, and if, as already mentioned, the channel width or friction had

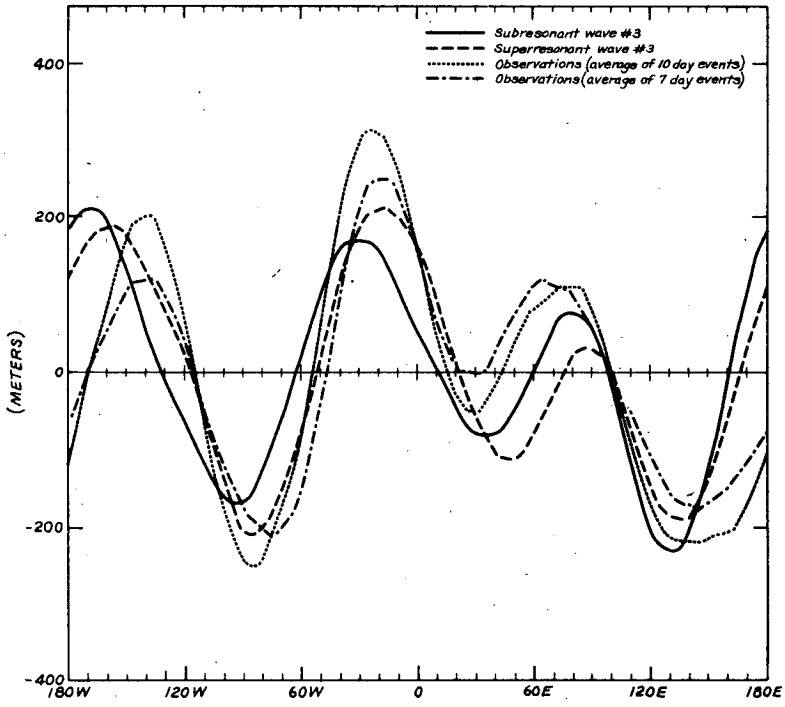

FIG. 18. Subresonant and superresonant wavenumber 3 solutions and average of all events in Fig. 11 and Fig. 16.

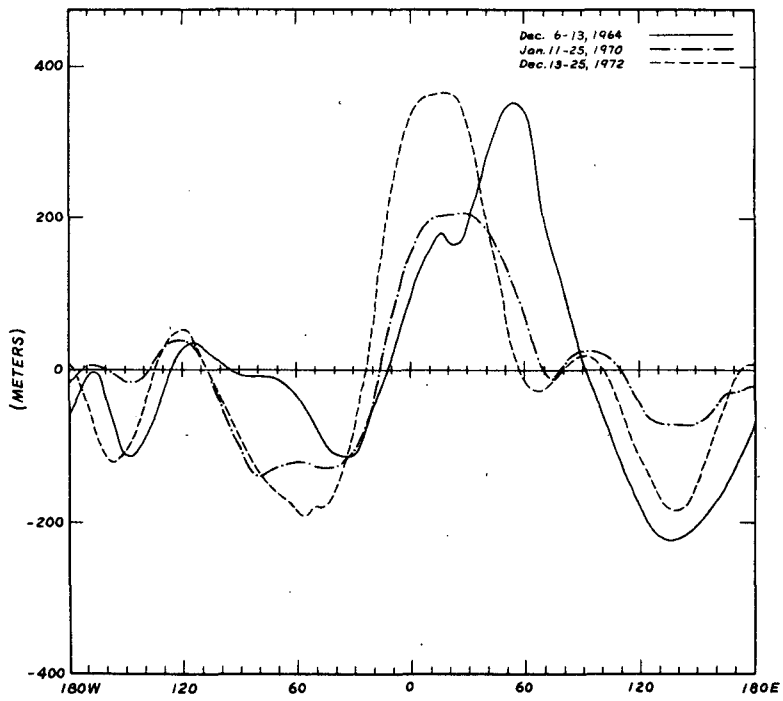

FIG. 19. As in Fig. 15 except dominated by wavenumber 1.

also been reduced, wavenumber 1 equilibria also would have become possible. Fig. 21 shows the remaining four events which could not be identified with other patterns and for which we do not have analytical counterparts.

6. Conclusions

We offer the following interpretation of our results as a possible explanation of blocking phenomena. First, we remark that the momentum driv-

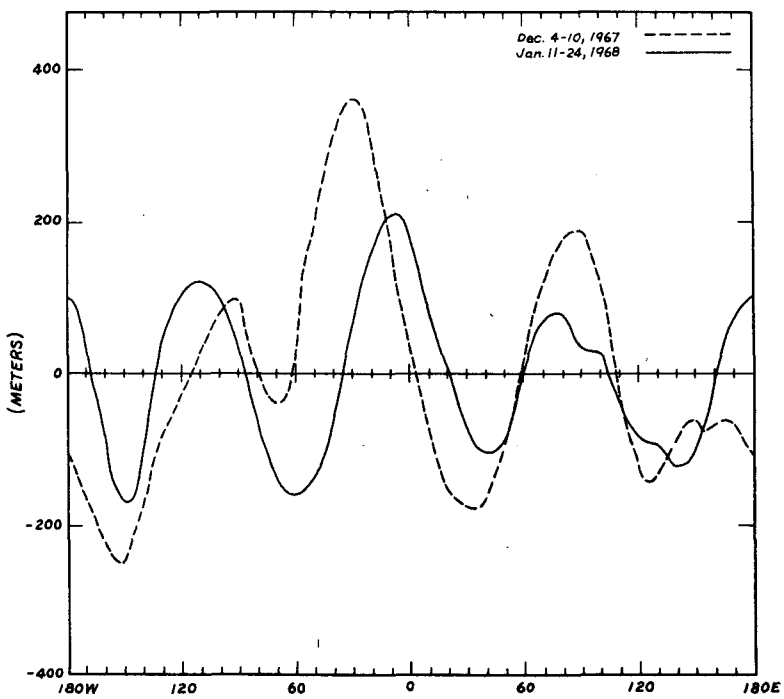

FIG. 20. As in Fig. 15 except dominated by wavenumber 4.

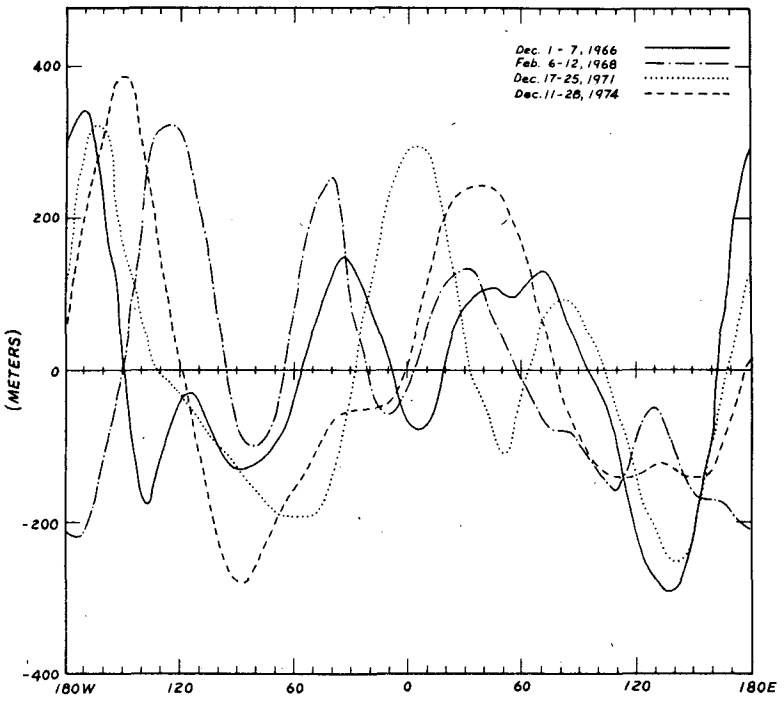

FIG. 21. As Fig. 15 except without analytical counterparts.

ing, ψ^* in Eq. (1) or U^* in Eq. (3), was prescribed so as to give as one of the multiple equilibria that which was determined in CE as closest to the normal or climatological field for January. This choice is justifiable only if, despite the occurrence of a multiplicity of accessible equilibrium states, one of these so dominates that the normal pattern resembles this state. If this were not the case, the driving would be arbitrary, and the arbitrariness could be eliminated only by employing a baroclinic model in which the actual thermal driving of the atmosphere could be introduced. Since the assumed momentum driving in the barotropic model is a substitute for this thermal driving, we must expect that it, like the thermal driving, will not be zonally uniform or even fixed in time. A longitudinally variable driving would give preference to certain longitudes for ridge or trough intensification and could therefore account, at least in part, for the regional character of observed blocking configurations (greater amplitude of one of the several ridges or troughs at a given latitude). We remark also that a uniform increase of U^* in Fig. 2 would drive the flow closer to resonance and thereby increase the amplitude of the normal (subresonant wavenumber 2) pattern until it became a large-amplitude blocking pattern. There is evidence from a treatment of baroclinic flows (Charney and Straus, 1980) that such a flow also would become more stable. This circumstance provides a possible explanation for the well-known fact that many blocking patterns appear merely as an amplification of the normal pattern. Finally, we point out that allowing space and time variations of driving and friction as well as variations in lateral extent enables wavenumber 1 and 4 resonances to occur and so provides a possible explanation for the observed wavenumber 1 and 4 blocking patterns, which are not presently included in our model.

The present model produces equilibria which resemble 8 of the 14 strongly persistent blocking events listed in Table 2 (four subresonant wavenumber 2 configurations and four wavenumber 3 configurations) and 11 of the 20 less persistent events listed in Table 3 (three subresonant wavenumber 2 configurations and eight wavenumber 3 configurations). If one now adds the three wavenumber 1 and the two wavenumber 4 configurations, which could be obtained by a slight extention of our model, one finds that a total of 24 of 34 events are at least potentially explainable as quasi-steady equilibrium configurations in our model.

It sometimes happens that blocking ridges occur simultaneously in the Pacific and the Atlantic. By subtracting the normal flow pattern (dotted curve in Fig. 3) we obtain the anomaly pattern, and it may be seen that the 7–13 January 1971 event in Fig. 15, as well as several more events if the amplitude criterion is reduced to 100 gpm, have simultaneous blocks in the Pacific and the Atlantic. These cases are explainable simply as wavenumber 2 or 3 resonances for a zonally uniform driving near resonance.

The regional character of block formation is not explained by our model. However, we may suggest that the inclusion of longitudinal variations of external forcing and dissipation might possibly account for this property. Other approaches are possible. Multiple equilibria are found near critical Froude numbers in hydraulic flow over isolated obstacles (Baines and Davies, 1980), and these are associated with the occurrence of shock phenomena. The question arises: can flow over a localized obstacle produce quasi-geostrophic multiple equilibria? In the hydraulic jump case the flow becomes unstable at the critical Froude number where the group velocity of (the nondispersive) long gravity wave vanishes, and it is the vanishing of the group velocity, not the vanishing of phase velocity, that one must consider in dealing with the instability of flow over an isolated, as distinguished from a sinusoidal, obstacle. Analogously, in the case of quasi-geostrophic β-plane flow over an isolated two-dimensional obstacle, Lee-Or Merkine (private communication) has found that a nonpropagating localized orographic instability sets in when the group velocity of the disturbance wave packet at the obstacle becomes zero. The search for such instabilities and their possible development into multiple equilibria may very well require more lateral y structure than is presently allowed in our model.

The second phenomenon that we have failed to explain by our model is the mechanism of transition from normal to blocking situations and vice-versa. As we have already suggested, the generation or decay of a block may occur by a change of external driving so as to drive the zonal flow closer to or farther from resonance. Changes of this kind would presumably be produced by factors not included in our model, such as synoptic-scale wave-mean flow interactions or variable heating depending on the motion. A block may be initiated by a deep cyclonic storm development which locks the flow pattern into a blocking equilibrium or, vice versa, when it drives the flow out of a blocking equilibrium. If the changed driving causes the flow to enter a superresonant blocking state, form-drag instability (Charney and DeVore, 1979; Charney and Straus, 1980) will transform it into a subresonant equilibrium. Finally, the blocking configuration may be unstable to traveling waves. Charney and Straus (1980) found for the two-layer baroclinic case with sinusoidal topography that a given thermal driving may produce a blocking configuration which is unstable to propagating waves having the same zonal wavenumber. These modes may be periodic, nonperiodic but recurrent, or random. The nonrecurrent planetary-scale waves may destroy the blocking pattern, as may also its synoptic-scale baroclinic instabilities.

In the second part of this paper we consider a thermally driven two-layer baroclinic model. The equilibrium configurations are found to be similar to those of the barotropic model for appropriate thermal driving. However, the mechanisms for their maintenance and the character of their instabilities are quite different. Baroclinic instability plays an important role.

REFERENCES

Baines, P. G., and P. A. Davies, 1980: Laboratory studies of topographic effects in rotating and/or stratified fluids. GARP Publ. Ser., No. 23, 235–301.

Charney, J. G., and A. Eliassen, 1949: A numerical method for predicting the perturbations of the middle latitude westerlies. *Tellus*, **1**, 38–54.

——, and J. G. Devore, 1979: Multiple flow equilibria in the atmosphere and blocking. *J. Atmos. Sci.*, **36**, 1205–1216.

——, and D. M. Straus, 1980: Form-drag instability, multiple equilibria and propagating planetary waves in baroclinic, orographically forced, planetary wave systems. *J. Atmos. Sci.*, **37**, 1157–1176.

Derome, J., and A. Wiin-Nielsen, 1971: The response of a middle latitude model atmosphere to forcing by topography and stationary heat sources. *Mon. Wea. Rev.*, **99**, 564–576.

Dole, R. M., 1978: The objective representation of blocking patterns. *The General Circulation: Theory, Modeling and Observations*, Notes from a Colloquium: Summer, 1978. NCAR/CQ – 6 + 1978 – ASP, pp. 406–426.

Hart, J. E., 1979: Barotropic quasi-geostrophic flow over anisotropic mountains. *J. Atmos. Sci.*, **36**, 1736–1746.

Namias, J., 1978: Multiple causes of the North American abnormal winter 1976–77. *Mon. Wea. Rev.*, **106**, 279–295.

Rex, D., 1950: Blocking action in the middle troposphere and its effect upon regional climate. I. An aerological study of blocking action. *Tellus*, **2**, 196–211.

Shukla, J., and B. Bangaru, 1980: Effect of a Pacific sea-surface temperature anomaly on the circulation over north America: A numerical experiment with the GLAS model. GARP Publ. Ser., No. 22, 501–518.